

BENCHMARK ANALYSIS OF THERMAL STRIPING PHENOMENA IN PLANAR TRIPLE PARALLEL JETS TESTS FOR FUNDAMENTAL VALIDATION OF FLUID-STRUCTURE THERMAL INTERACTION CODE FOR SODIUM-COOLED FAST REACTOR

Masaaki Tanaka

Japan Atomic Energy Agency,
4002 Narita-cho, O-arai, Ibaraki 311-393, Japan
tanaka.masaaki@jaea.go.jp

Kazuyoshi Nagasawa

NESI In-corporation,
4002 Narita-cho, O-arai, Ibaraki 311-393, Japan

ABSTRACT

Thermal striping may be caused in the region where temperature fluctuation is induced by mixing of fluids at different temperatures. Since it may cause high cycle thermal fatigue in structure and affect the structural integrity of the component in a power plant, thermal striping is one of the most important issues in the design of the sodium-cooled fast reactors (SFRs). In JAEA, a series of the water experiments (WAJECO) and the sodium experiment (PLAJEST) for planar triple parallel jets mixing had been performed to investigate the mixing process of the jets and the attenuation process of the temperature fluctuation from fluid to structure. In order to estimate the structural integrity against the thermal fatigue, the author has developed a numerical simulation code named MUGTHES, which can deal with conjugate heat transfer between the fluid and the structure regions. For the fundamental validation of MUGTHES, numerical simulations for the planar triple parallel jets tests in WAJECO and PLAJECT have been conducted through the benchmark analysis. According to the proposal of benchmark specifications, the information on the experimental conditions including geometry data and the experimental results were provided. In the numerical simulations by MUGTHES, the thermal interaction between fluid and structure was simulated and the large eddy simulation (LES) approach with the standard Smagorinsky model was employed to simulate large-scale eddy motion in the mixing region. In comparison between the numerical results and the experimental results, thermal mixing process and large-scale eddy structures in the triple jets and the relation between temperature fluctuation generation and large-eddy structures were revealed. And also, the attenuation process of temperature fluctuation from the fluid to the structure was indicated.

KEYWORDS

Benchmark analysis, Thermal striping, Fluid-structure thermal interaction simulation, Sodium-cooled Fast Reactor, Large eddy structure.

1. INTRODUCTION

High cycle thermal fatigue caused by thermal mixing phenomena has been one of the most important issues in the design of an advanced sodium-cooled fast reactor the Japan Sodium cooled Fast Reactor (JSFR) [1]. In the reactor, the perforated plate called as the Core Instruments Plate (CIP) is installed at the bottom of the Upper Internal Structure (UIS) in order to support thermocouples and the other sensors for

operations and safety measures [2]. Below the CIP, hot sodium comes from fuel assemblies and cold sodium flows out from control rod channels and blanket fuel assemblies located in the outer region of the core. When the fluid temperature fluctuation is transmitted to the CIP surface, cyclic thermal stress may be induced on the CIP, the upper guide tubes and the driving system of control rods. Such a cyclic stress may cause the crack initiation and crack growth in those structures depending on the frequency characteristics and the amplitude of the temperature fluctuation.

Since it is difficult to conduct the large scale experiments covering the JSFR operation conditions, establishment of numerical estimation methods for the high-cycle thermal fatigue in the JSFR is strongly desired. A numerical simulation code (MUGTHES), therefore, has been developed to investigate and estimate the high-cycle thermal fatigue in structure [3]. In developments of the numerical simulation code and the numerical estimation method, verification and validation (V&V) study is indispensable to make successful estimation of the thermal fatigue issue in the JSFR design. Tanaka [4] proposed a V&V procedure named V2UP (Verification and Validation plus Uncertainty quantification and Prediction) including uncertainty quantification and prediction for the multi-dimensional simulation. In the V2UP, the problems and experiments contributing to the V&V were categorized into four elements: the fundamental problems (FPs), the separated effect tests (SETs), the component effect tests (CETs), and the integrated effect tests (IETs). A fundamental problem (FP) basically contains a single element phenomenon in order to confirm applicability of the numerical schemes and the potential of the physical model for the numerical estimation of the target issue. The separated effect test (SET) should contain several elemental phenomena to check applicability of the numerical schemes and the physical models to the practical problems related to the target issue. The CETs and the IETs should be designed respectively to provide data on partial effects and synergistic effects of the phenomena in the target issue in the target plant. In the V2UP, the fundamental validation consisting of the FPs and the SETs and the validation consisting of the CETs and the IETs are separately defined. Through the fundamental validation consisting of the FPs and the SETs, potential capability of the numerical simulation code for the target issue is to be confirmed. Through the validation consisting the CETs and IETs, comprehensive capability of the numerical simulation codes and methods for the prediction is to be confirmed.

In this study for the thermal fatigue estimation in the JSFR, the benchmark simulations of PLAJECT and WAJECO appearing in this paper are positioned in the category of the SET. A number of experiments of the water (WAJECO) and the sodium (PLAJEST) tests for planer triple parallel jets mixing had been conducted in JAEA [7-9]. Through the experiments, the mixing behavior of the jets at different temperatures and the attenuation process of the temperature fluctuation from the fluid to the structure had been investigated. The water experiment WAJECO had almost the same configured test section with the sodium experiment PLAJECT. Through the benchmark simulations, thus, applicability of MUGTHES to the thermal striping phenomena due to mixing of the jets at different temperatures are to be confirmed in the viewpoint of the numerical schemes, the turbulence model for the unsteady motion of large scale eddies and conjugate heat transfer model. And the potential capability of MUGTHES to the utilization for the thermal fatigue issue in the JSFR is to be confirmed.

One note that this benchmark [6] has been performed under the auspices of an international collaboration on thermal hydraulics for sodium-cooled fast reactor development with participation from the Japan Atomic Energy Agency (JAEA), the U.S. Department of Energy (USDOE), and the French Commissariat à l'énergie atomique et aux énergies alternatives (CEA) [10].

2. OUTLINE OF NUMERICAL SIMULATION

2.1 Outline of MUGTHES code

MUGTHES employs the LES approach to predict unsteady thermal mixing phenomena and the boundary fitted coordinate (BFC) system to fit complex boundary shapes in a reactor [3]. Two calculation modules of the thermal-hydraulics module to calculate velocity and fluid temperature and the structure module to analyze unsteady heat conduction in structure are employed. A finite volume approach and

finite differential schemes [11] are used to solve the unsteady incompressible Navier-Stokes equation and energy conservation equation in the thermal-hydraulics module and the unsteady heat conduction equation in the structure module. A collocated grid system is employed so that the physical velocity components (u, v, w) in the Cartesian coordinate system, the pressure and the temperatures of fluid and structure are defined at the center of computational cell. In the BFC system, additional terms of the Jacobian J and surface area vectors are evaluated based on the finite volume approach [3]. The central differential scheme is used in the equations except an advection term in the energy conservation equation. The Crank-Nicolson method is used for time integration and the Projection method [12] is used to solve velocity field. Specifications of the numerical models for the benchmark were listed in Table 1.

2.2 Large Eddy Simulation Approach

The turbulent viscosity μ_t in the code is evaluated by the standard Smagorinsky model (SSM) [13] as follows.

$$\mu_t = \rho(C_s f \Delta)^2 |D| \quad (1)$$

$$f = 1 - \exp(-\delta^+ / 25) \quad (2)$$

$$\Delta = J^{1/3} \quad (3)$$

$$|D| = \sqrt{2D_{ij}D_{ij}}, \quad D_{ij} = (\partial u_i / \partial x_j + \partial u_j / \partial x_i) / 2 \quad (4)$$

Here, C_s is the parameter coefficient of the model and Δ is the filter length evaluated with the Jacobian J corresponding to the cell volume. D_{ij} is the rate of strain tensor defined at the cell center in the BFC system. In boundary cells on wall, van Driest damping function in Eq. (2) is used. Since our goal is to numerically estimate unsteady thermal-hydraulics and thermal fatigue in the large-scale system JSFR, artificial wall conditions [14] derived by a wall function law [15] are considered in the LES approach in order to utilize a coarse mesh arrangement near wall region suppressing computational load for a long time transient calculation in the system [3]. By using the wall function law, the wall shear stress in the diffusion term and the velocity gradient for the SSM are estimated in the coarse mesh arrangement.

2.3 Temperature Field in Conjugate Heat Transfer Problem

After velocity field is calculated, the fluid temperature is calculated solving the unsteady energy equation of the flow field with the velocity components at a new time step in the thermal-hydraulics module and the structure temperature is also calculated solving the unsteady heat conduction equation in

Table 1 Numerical Conditions of MUGTHES for benchmark simulation

Numerical method	Projection method and Crank-Nicolson scheme with finite volume approach and finite differential method in collocated grid system	
Discretization scheme in advection term	(momentum)	2nd order central differential
	(energy)	Higher-order upwind scheme with oscillation control technique
Pressure matrix solver	BiCGSTAB combined with Jacobi method	
LES model:	Standard Smagorinsky Model with van Driest function ($C_s=0.14$)	
Wall function:	3 Layer model (Viscous sub layer, Buffer layer, Log-law)	
Thermal diffusion	MILES approach (implicit LES without physical model)	
Thermal interaction	Conjugated heat transfer with Myon-kasagi correlation	
Parallel computing	SPMD (thread parallel with OpenMP)	

the structure module. In the thermal-hydraulics module, the monotone integrated large eddy simulation (MILES) approach [16] which has been successfully used in numerical simulations of thermal striping phenomena [17-19] is employed without the explicit thermal diffusion model and a higher order accuracy upwind scheme [20] with a simple limiting procedure is used for the advection term in the energy equation [3]. In the thermal interaction problem, the structure and the fluid temperatures are calculated through the surface temperature on the boundary of both fields which is iteratively solved by a conjugated heat transfer model based on the Fourier's law as follows:

$$q_s + q_f = \lambda^*_f \frac{\partial T_f}{\partial (x_n)_f} + \lambda_s \frac{\partial T_s}{\partial (x_n)_s} = 0 \quad (5)$$

Subscripts of f and s respectively mean variables respectively belonging to the fluid and the structure regions. T is temperature and x_n is the normal axis to the wall surface. λ_s (W/m/K) is heat conduction of structure. Effective heat conduction of fluid λ^* ($=\lambda_f+\lambda_t$) (W/m/K) is the sum of molecular heat conduction of fluid λ_f and heat conduction by turbulence diffusion λ_t ($=\alpha_t/(\rho_f C_{p_f})$). Turbulence temperature diffusion coefficient α_t ($=\nu_t/Pr_t$) is estimated with the fluid density ρ_f (kg/m³) and heat capacity of fluid C_{p_f} (J/kg/K). Turbulent eddy viscosity ν_t is derived by the SSM. Turbulent Prandtl number Pr_t is given by the following equation [21] with a local Prandtl number of fluid Pr .

$$Pr_t = 0.75 + 1.63 / \left[\ln \left\{ 1 + (Pr/0.0015) \right\} \right] \quad (\text{for } 10^{-2} < Pr < 5 \times 10^4 \text{ and } 10^4 < Re < 10^5) \quad (6)$$

3. OUTLINE OF BENCHMARK CONDITIONS

3.1 Computational Domain

Figures 1 (a) and (b) show the mesh arrangements on the vertical planes in parallel and perpendicular to the test plate surface, respectively. Figure 1 (c) shows dimensions of the test section as a recommended computational domain proposed by Kobayashi et al. [6]. Grey colored part shows the test plate in which

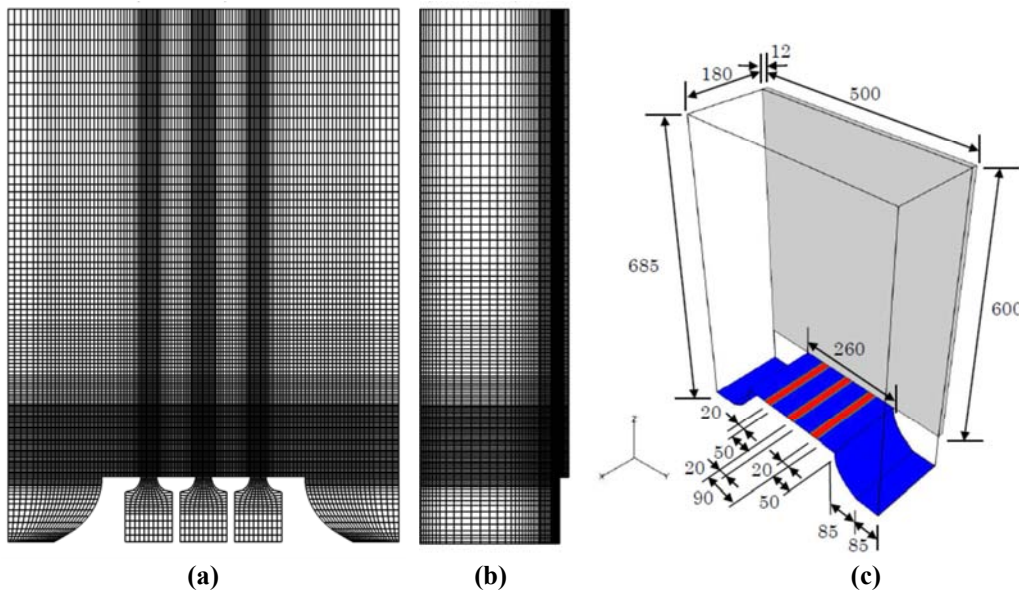


Fig. 1 Mesh arrangements on the vertical cross sections in (a) parallel and (b) perpendicular to the test plate surface and (c) dimensions of a recommended computational domain [6].

thermal interaction must be concerned, red colored area shows outlets of the discharged nozzles, and blue colored area shows the bottom boundary of the test section in PLAJECT. Since MUGTHES can solve the fluid and the structure regions simultaneously, computational meshes for two regions are arranged in one domain. Right side meshes shown in Fig. 1 (b) as a thin part attached to the fluid region are for the test plate. On the boundary between both regions, thermal interaction is considered through the wall temperature derived by the conjugated heat transfer model by Eq. (5) on the the common mesh arrangement. The minimum cell size in depth direction (x) appears on the boundary between fluid and structure regions and is 1 mm and 0.5 mm for the fluid and the structure regions, respectively. In order to simulate the true penetration behavior of temperature fluctuation in the structure, the smaller mesh is required to solve the higher frequency component of temperature fluctuation. And such a fine mesh arrangement requires a huge computational load for transient calculation. High frequency component, however, have less impact on the structural integrity. Therefore, introduction of a threshold value to the mesh size can be a practical modification [22]. The minimum mesh size of 0.5 mm for the structure is estimated by considering penetration characteristics of temperature fluctuation in the structure and temperature fluctuation up to 10 Hz may simulate in the structure with this mesh [22]. The minimum mesh size in horizontal (y) and vertical (z) directions is 2 mm in both regions around the jet outlets. Total cell numbers are 650,664 and 141,240 for the fluid and the structure regions.

Dimensions of computational domain are set according to the benchmark specifications proposed by Kobayashi, et al. [6] shown in Fig. 1 (c). Dimensions of fluid region are of 180 mm in depth, 500 mm in horizontal direction and 685 mm in the vertical direction from the bottom of the test section. As for the metal plate, dimensions are of 12 mm in depth, 500 mm in horizontal direction and 600 mm in the vertical direction from the outlet of the nozzle.

Table 2 Experimental Conditions Proposed for Benchmark Simulation

Case	Outer-slits/Hot jets		Center-slit/Cold jet		Index of mixture		
	V_h (m/s)	T_h (°C)	V_c (m/s)	T_c (°C)	V_m (m/s)	ΔT (°C)	T_m (°C)
A1 (SJ3-A05) ^{*1)}	0.51	347.5	0.51	304.5	0.51	43	333.2
A2 (WJ4s-A01) ^{*2)}	0.48	40.3	0.48	32.0	0.48	8.3	37.5
B1 (SJ3-A11) ^{*3)}	0.51	349.8	0.32	311.0	0.45	38.8	340.5

*1) NUTHOS-7 [8] and NURETH-11 [7], *2) NURETH-12 [9], *3) NURETH-11 [7]

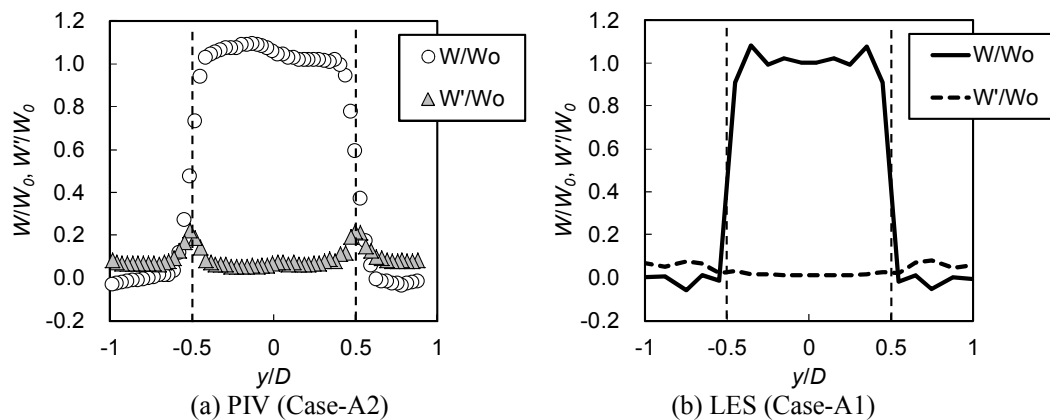


Fig. 2 Horizontal profiles of the time average W/W_0 and the fluctuation intensity W'/W_0 of axial velocity component near the center nozzle outlet in the middle of the test section, comparing with the PIV results in Case-A2.

3.2 Boundary Conditions

Table 2 shows boundary conditions for the benchmark simulation. Case-A1 (sodium) is an iso-velocity condition in PLAJECT and Case-A2 (water) is also an iso-velocity condition in WAJECO. In order to investigate the influence of the difference of the fluid between sodium and water, both cases were employed. Case-B1 as an aniso-velocity condition in PLAJECT was also employed, in order to investigate the influence of the unbalance of the discharged velocities at the nozzle outlets.

In fluid region, the non-slip condition was set on the bottom surface (blue colored area shown in Fig. 1 (c)) and the free-slip condition was set on side surfaces. On the top surface, convective outflow was set as outlet conditions. As for the inlet condition, uniform profile of axial velocity without fluctuation was set on the bottom surfaces of the nozzle chamber to achieve the discharged velocities listed in Table 2. Nozzle chambers don't appear in Fig. 1 (c), but did in Fig. 1 (a). The constant fluid temperature was set on the bottom surfaces of the nozzle chamber according to the values in Table 2. Adiabatic condition was set on the surfaces of the domain, except bottom surfaces of the nozzle chamber and the test plate surface on the side of the fluid region. The conjugate heat transfer condition by Eq. (5) was set on the boundary surface between the fluid region and the test plate.

Figure 2 shows the horizontal profiles of the time average W/W_0 and the fluctuation intensity W'/W_0 of axial velocity component in Case-A1 (sodium), compared with those of the PIV results in Case-A2 (water). By considering the nozzle chambers in upstream of the discharged nozzle, horizontal velocity profiles of the time averaged axial velocity could be simulated though the magnitude of the fluctuation intensity showed the relatively small value.

Transient calculation with a time interval of $\Delta t = 0.2$ ms was conducted in 200,000 steps and the latest 10,000 data for 20 seconds (sampling rate at 500 Hz) were used for the post-analysis. Coefficient of the SSM was 0.14 ($=Cs$) based on the experiences of T-pipe simulation [3, 22, 23].

4. NUMERICAL RESULTS

4.1 Comparisons with Experimental Results

4.1.1 Horizontal profiles of axial velocity component

Figures 3 (a), (b) and (c) show horizontal profiles of the time average W/W_0 and the fluctuation intensity W'/W_0 of axial velocity component at $z/D=5$ at the middle of the test section, in Case-A1 (Sodium), Case-A2 (Water) and Case-B1 (sodium), respectively. In iso-velocity cases of Case-A1 and Case-A2, velocity profiles of the time average and the fluctuation intensity in both cases were very similar to each other and they agreed with the PIV measurements in Case-A2. From the results in Figs. 3

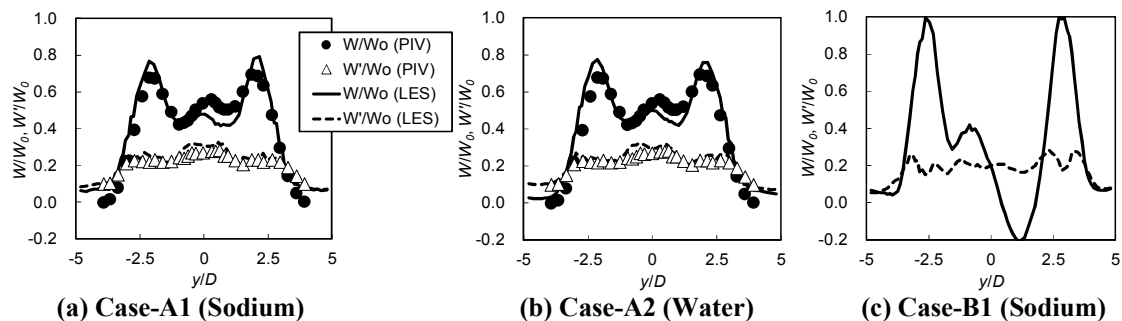


Fig. 3 Horizontal profiles of time average and fluctuation intensity of axial velocity component at $z/D=5$ in Case-A1, Case-A2 and CaseB1 at the middle of the test section ($x/D=4.5$), comparing with the PIV result in Case-A2.

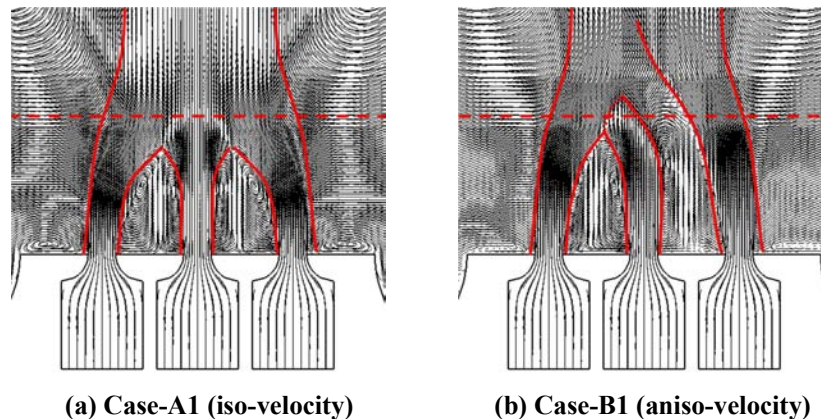


Fig. 4 Flow patterns drawn by the stream lines in the triple jets mixing at the middle of the test section ($x/D=4.5$).

(a) and (b), it could be indicated that the weak fluctuation at the nozzle outlet as shown in Fig. 2 (b) didn't affect the mixing behavior in the downstream. In Case-B1 as aniso-velocity case, velocity profile was quite different from that in iso-velocity case.

Figures 4 (a) and (b) show flow patterns drawn by the stream lines in the time average field of the triple jets mixing at the middle of the test section ($x/D=4.5$). The dotted red line in the figures shows the position at $z/D=5$ as the same position as shown in Fig. 3. True red lines in the figures show the expected boundary lines of the jets to support to understand the flow pattern. Nouali and Mataoui [24] indicates that the triple jet flow can be categorized into four patterns due to the magnitude of the ratio of the side jet to the central jet velocities defined by $V_r (=V_h/V_c)$. While the flow pattern is symmetrical to the center of the center jet when V_r is less than 1.11, the asymmetric flow pattern can be observed in the $1.2 < V_r < 2$. As $V_r = 1$ in Case-A1 and Case-A2, the horizontal profiles as shown in Figs. 3 (a) and (b) are symmetrical. On the other hand, the horizontal profile as shown in Fig. 3 (c) is asymmetric because of $V_r = 1.59$ in Case-B1. The center jet at low temperature bends to the left side jet ($y/D < 0$). Therefore, the local higher peak of the axial velocity at $y/D = -0.88$ is shown because the core of the center jet exists there and the reverse flow is shown in opposite side at $y/D = 0.88$. These flow patterns can be seen in Fig. 4 (b) and are consistent with the results of the flow pattern categorized by the velocity ratio of V_r . The velocity ratio V_r can be an important factor in the mixing phenomena of the triple jets.

4.1.2 Horizontal profiles of fluid temperature in the mixing region

Figures 5 (a), (b) and (c) show horizontal profiles of the time average and the fluctuation intensity of the fluid temperature at $z/D=5$ and at (1) the middle position between the walls and (2) near wall position (1 mm from the wall) in Case-A1, Case-A2, and Case-B1, respectively. In iso-velocity cases of Case-A1 and Case-A2, the horizontal profiles of the time average and the fluctuation intensity of the fluid temperature were symmetric to the center line of the center jet as the same trend in the axial velocity profiles. In aniso-velocity case of Case-B1, the horizontal profiles of the time average and the fluctuation intensity of the fluid temperature were asymmetric to the center line of the center jet as the same trend in the axial velocity profiles. In all cases, temperature fluctuation intensity was high on both sides of the central jet (at $\pm y/D=0.75$ in iso-velocity cases) and magnitude of the intensity was less than 30 % of the temperature difference of ΔT . Temperature fluctuation could be actively caused between the side jet and the center jet. The numerical results of MUGTHES almost agreed with the experimental results and could trace well the trends of the experimental results.

4.2 Characteristics of Temperature Distributions from Fluid to Structure

distributions to the center of the domain were shown in Case-A1 and Case-A2 as iso-velocity conditions. In an aniso-velocity condition of Case-A2, temperature fluctuation distribution was asymmetric to the center. However, asymmetric distribution gradually dissolved from the middle region as shown in Fig. 6 (c-1) to the wall surface as shown in Fig. 6 (c-3) and almost symmetric distribution appeared in the structure as shown in Fig. 6 (c-4). Distributions in Case-A1 (sodium) and Case-A2 (water) were almost the same in the middle position as shown in Figs. 6 (a-1) and (b-1). However, those in near wall regions as shown in Figs. 6 (a-2) and (b-2), wall surfaces as shown in Figs. 6 (a-3) and (b-3) and in the structures

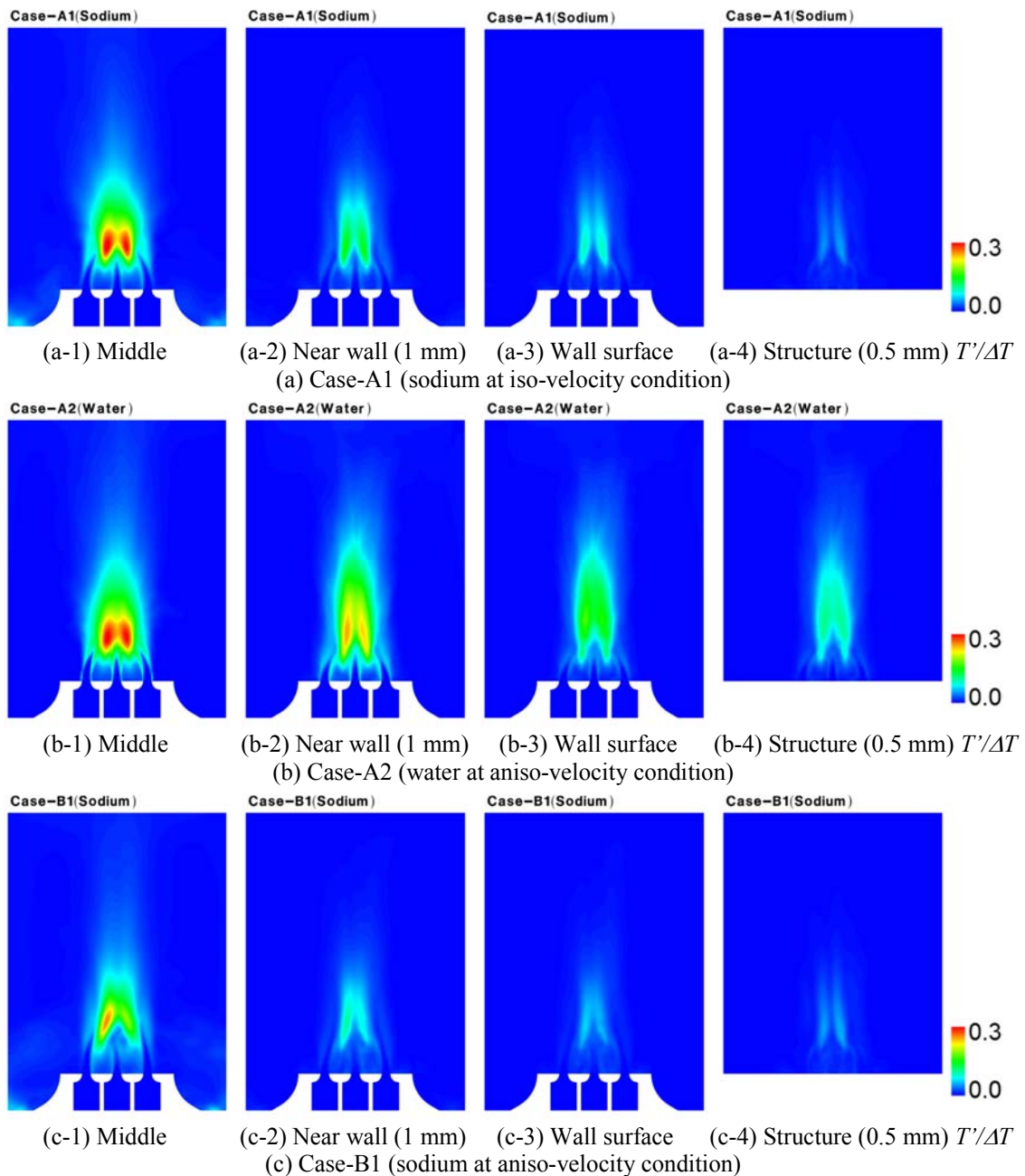


Fig. 6 Distributions of fluid temperature fluctuation intensity on the vertical plane.

as shown in Figs. 6 (a-4) and (b-4) were slightly different each other, in the viewpoint of the expansion of the fluctuation intensity. Temperature fluctuation intensity in Case-A1 (sodium) was lower than that in Case-A2 (water). In this sense, conservative estimation for the thermal striping and high cycle thermal fatigue could be made when it was only based on the results of the water experiment or of the numerical simulation of the water experiments. Although the water experiments are easy to work with, sodium experiments should be performed for the thermal striping phenomena in the case that the thermal interaction between fluid and structure should be considered, for the sodium-cooled fast reactor.

4.2.2 Temperature profiles from fluid to structure along normal direction to the wall

Figures 7 (a) and (b) show the profiles of the temperature fluctuation intensity at $z/D=5$ and $y/D=\pm 0.75$ along the depth direction from the fluid to the structure in Case-A1 and Case-A2. Although the magnitude of the fluctuation intensity derived by the numerical simulation was higher than that of the experimental results in the middle region at $x/D\sim 4.5$, numerical results were lower than that of the experimental results in Case-A1 (sodium) near the wall. The temperature fluctuation generation near wall surface and heat transfer has deep relations with the behavior of the eddy structures as mentioned in the next section. Characteristics of the fluid temperature fluctuation generation near wall region are different from those in the middle region far from the wall.

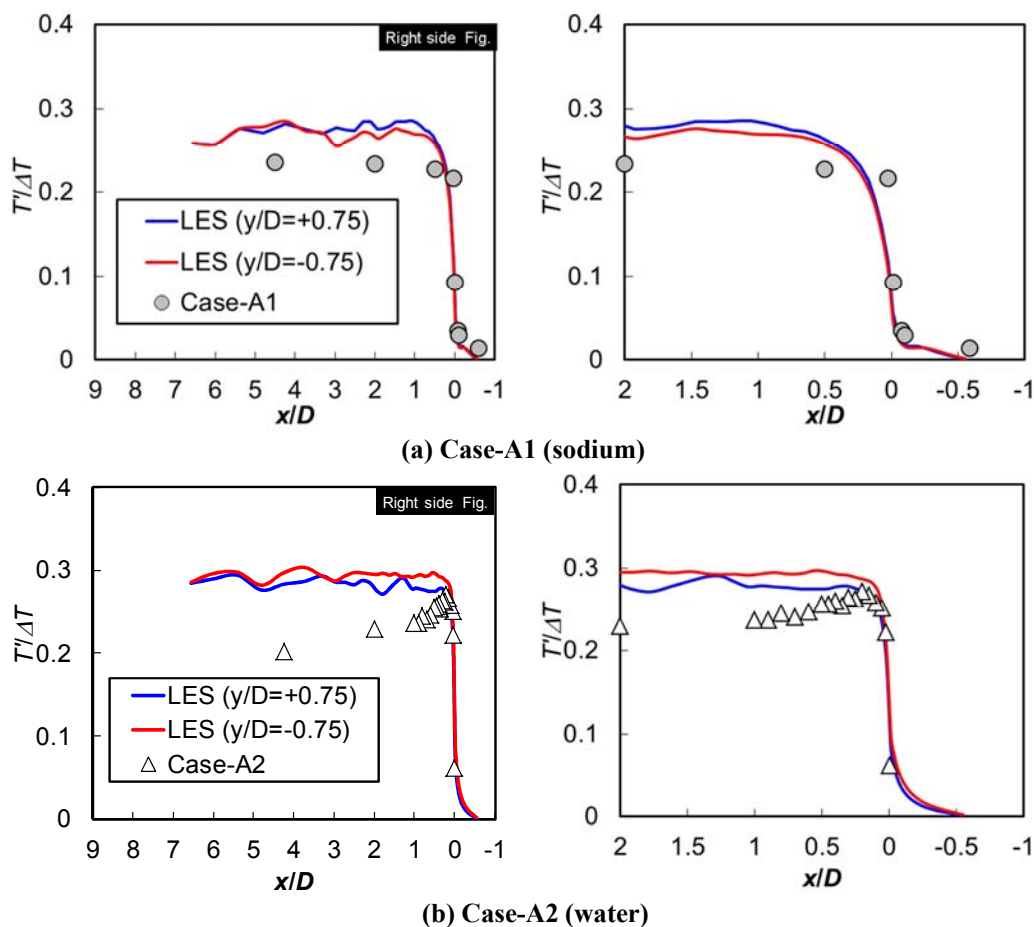


Fig. 7 Temperature fluctuation intensity at $z/D=5$ and $y/D=\pm 0.75$ along depth direction from fluid to the inside of structure.

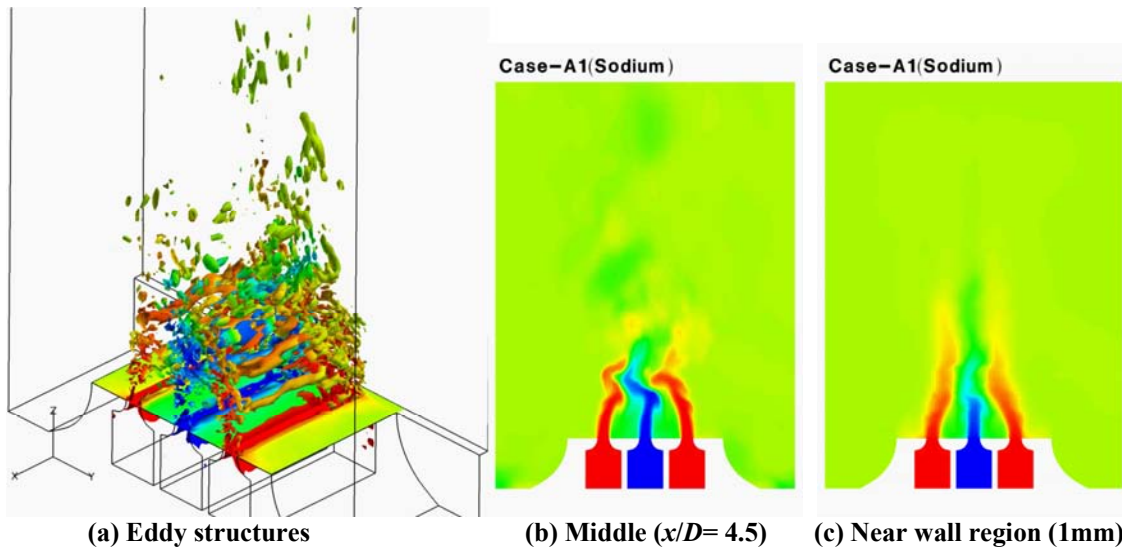
4.3 Characteristics of Temperature Fluctuation Mitigation from Fluid to Structure

4.3.1 Characteristics of Eddy Structures in the Mixing Region

Figure 8 (a) shows the instantaneous eddy structures drawn by the iso-surface of the 2nd invariant of the velocity tensor at $Q=321.5 (=0.5 \times (W_0/D)^2)$ in Case-A1 at a typical time step. Figures 8 (b) and (c) show the instantaneous temperature distributions on the vertical cross sections at the middle of the test section and the 1 mm near the wall, at the same time step of Fig. 8 (a). As shown in Fig. 8 (a), eddy structures in the middle region between the walls and near wall region were quite different.

In the middle area of the test section as shown in Fig. 8 (b), large scale horizontal eddies parallel to the nozzle edge are shown because the shear force to form such a large scale eddy is generated alongside of the nozzle outlet. Due to the periodic motion of the large eddy structures, a pair of the center jet and the left side jet bends to the right side, and the right side jet bends to the left side. After approximately 0.2 seconds, a pair of the center jet and the right side jet bends to the left side, and the left side jet bends to the right side. These cyclic motions continue in the mixing region. Therefore, swing motion of the center jet at 2.3 Hz ($St=fD/W_0=0.09$) is shown. The dominant frequency corresponds to the experimental results as shown in Fig. 9 in the next section.

On the contrary, in the near wall region, small eddies are generated by the shear force between the wall surface and the vertical flow of the jets. Axis of such a small eddy has horizontal direction in parallel to the wall surface according to the shear direction caused by the vertical jet flows. As shown in Fig. 8 (c), swing motion of the center jet is weakened in the near wall region. Suppression of the swing motion of the center jet decreases the low frequency components of the temperature fluctuation in fluid, but small eddies cause the high frequency components of the temperature fluctuation in fluid. The structure does not respond to the high frequency components of temperature fluctuation because of its high thermal diffusivity. Thus, the temperature fluctuation transfer is mitigated near wall region as total. This is recognized as the boundary layer effect. Therefore, fine mesh should be arranged near wall region to simulate the small eddy structures. Since very high frequency components of temperature fluctuation don't have much impact on the thermal stress in the structure, threshold of the mesh size may exist in the numerical simulation. As the future work, appropriate mesh size will be investigated considering the impact on the thermal stress in the structure.



(a) Eddy structures (b) Middle ($x/D=4.5$) (c) Near wall region (1mm)
Fig. 8 Instantaneous temperature distribution related to the eddy structure drawn by the iso-surface of the 2nd invariant of the velocity tensor at $Q=321.5 (=0.5(W_0/D)^2)$ in Case-A1.

4.3.2 Power spectrum density of temperature fluctuation

Figures 9 (a) and (b) show the power spectrum density (PSD) profiles of temperature fluctuation in Case-A1 and Case-A2 respectively, at $z/D=5$ and $y/D=-0.75$ along the depth direction from the middle location of the test section ($x/D=4.5$) to the inside of the structure ($x/D=-0.0125$) through the near wall position in fluid ($x/D=0.025$). In the experiment, dominant frequency was 2.54 Hz in Case-A1 and 2.15 Hz in Case-A2 and the Strouhal numbers are 0.0996 and 0.0895, respectively. In the numerical simulation as show in Fig. 9 (a) and (b), the Strouhal numbers are 0.09 and 0.086 in Case-A1 and Case-A2, respectively. As the same with the experiment, the Strouhal number in Case-A1 (sodium) is slightly higher than that in Case-A2 (water). The reasons of this difference are not defined, yet. Since the dominant frequency is decided by the motion of the large scale eddy structure in the mixing region, one considers that the influence of the properties of fluid should be considered because liquid sodium has a small viscosity of the water.

4.4 Considerations through the Benchmark Simulations

Through the benchmark simulations using MUGTHES, it can be recognized that numerical results with the mesh arrangement shown in Fig. 1 can follow the experimental results and that the numerical models described in Sec. 2 are potentially applicable. As mentioned in Sec. 4.3.1, however, small eddy structures going up to the upper region along the wall surface were observed near wall region. This may indicate that the nature of flow structure near wall region in this system is different from that in the simple system such as the uniform flow on the flat plate, in which the wall function law is applicable. In MUGTHES, the wall shear stress and the velocity gradient in the boundary cell are estimated using wall function law [3]. Therefore, the limitation of this approach will be investigated through the GCI estimation (mesh sensitivity study). As mentioned in Sec. 1, the benchmark simulations in this paper were conducted as an activity for the SETs in V&V process of MUGTHES. In the fundamental validation step, uncertainty quantification of the numerical results through the Grid Convergence Index (GCI) estimation is required [4]. The author conducted the uncertainty quantification of the numerical simulation by MUGTHES for the thermal striping phenomena in a T-junction piping system through the grid convergence index (GCI) estimation [22]. As the next step, the GCI estimation will be conducted to this benchmark problem. The mesh arrangement shown in Fig. 1 will be as a reference one and finer and coarser meshes will be prepared. For the finer mesh arrangement, suggestions were obtained through the discussion in Sec. 4.2, the dense mesh arrangements were required in the areas between the side jets and

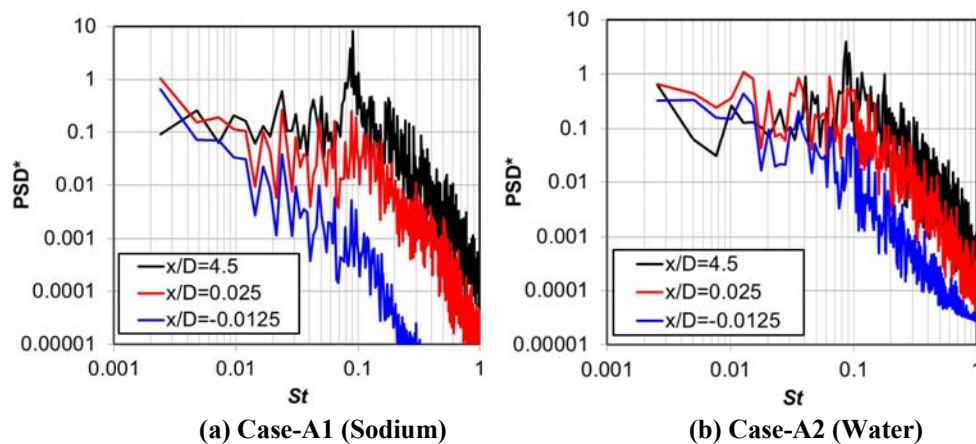


Fig. 9 The PSD profiles of temperature fluctuation at $z/D=5$ and $y/D=-0.75$ along depth direction from the middle location of test section ($x/D=4.5$) to inside of structure ($x/D=-0.0125$) through the near wall position in fluid ($x/D=0.025$).

the center jet, and from the nozzle outlet to the height position less than $z/D \sim 8$ where the parallel upward flows were recognized.

5. CONCLUSIONS

Numerical simulation for PLAJECT benchmark has been conducted by using thermal interaction simulation code MUGTHES. The LES with the standard Smagorinsky model was employed and transient temperature distributions of fluid and structure were simultaneously calculated by using conjugate heat transfer model. Numerical results almost agreed with the experimental results. Through the numerical simulation, several prospects to improve the accuracy of the numerical results were found in the viewpoint of the appropriate mesh arrangement. The relation between the thermal mixing process and the large-scale eddy structures in the triple jets mixing phenomena was revealed. The difference of characteristics of jets mixing in the areas of far from the wall and near the wall was clearly found and it depends on the motion of the eddy structures in each area. And also, the attenuation process of temperature fluctuation from the fluid to the structure near wall region was explained by the effect of the small eddy structures formed in the boundary layer on the wall. As the next step, the GCI estimation will be conducted for uncertainty quantification and the applicability of the numerical models will be checked for this benchmark problem.

REFERENCES

1. M. Ichimiya, et al., "A Next Generation Sodium-Cooled Fast Reactor Concept and Its R&D Program", *Nuclear Engineering and Technology*, **39**, 171-186 (2007).
2. K. Ohyama, O. Watanabe, H. Yamano, "Conceptual Design for Japan Sodium-Cooled Fast Reactor (2): Thermal-Hydraulic Design for Reactor Upper Sodium Plenum in JSFR", *Proc. of ICAPP '09*, Tokyo, Japan, May 10-14, Paper 9296 (2009). [CD-ROM]
3. M. Tanaka, H. Ohshima and H. Monji, "Thermal Mixing in T-Junction Piping System related to High-Cycle Thermal Fatigue in Structure", *J. Nuclear Science and Technology*, **48**(9), 790-801 (2010).
4. M. Tanaka, S. Ohno and H. Ohshima, "Development of V2UP (V&V Plus Uncertainty Quantification and Prediction) Procedure for High Cycle Thermal Fatigue in Fast Reactor ~ Framework for V&V and Numerical Prediction ~", *Proc. of the CFD4NRS5*, Zürich, Switzerland, Sep. 9-11 2014, S03-2 (2014).
5. G. E. Wilson, B. E. Boyack, "The Role of the PIRT Process in Experiments, code development and code applications associated with reactor safety analysis", *Nucl. Eng. Des.*, **186**, 23-37 (1998).
6. J. Kobayashi, M. Tanaka, S. Ohno and H. Ohshima and H. Kamide, "Proposal of Benchmark Problem of Thermal Striping Phenomena in Planar Triple Parallel Jets Tests for Fundamental Code Validation in Sodium-Cooled Fast Reactor Development", *Proc. of the NURETH-16*, Aug. 30-Sept. 4 2015, Chicago, USA, No. 13655 (2015).
7. N. Kimura, H. Miyakoshi, H. Ogawa, H. Kamide, Y. Miyake and K. Nagasawa, "Study on Convective Mixing Phenomena in Parallel Triple-Jet along Wall - Comparison of Temperature Fluctuation Characteristics between Sodium and Water -", *Proc. of NURETH-II*, Avignon, France, Oct. 2-6 2005, No. 427 (2005).
8. N. Kimura, H. Kamide, P. Emonot and K. Nagasawa, "Study on Thermal Striping Phenomena in Triple-Parallel Jet - Transfer Characteristics of Temperature Fluctuation in Sodium and Water based on Conjugated Numerical Simulation -", *Proc. of NUTHOS-7*, Seoul, Korea, October 5-9 2008, (2008).

9. N. Kimura, H. Kamide, P. Emonot and K. Nagasawa, "Study on Thermal Striping Phenomena in Triple-Parallel Jet - Investigation on Non-Stationary Heat Transfer Characteristics Based on Numerical Simulation -", *Proc. of NURETH-12*, Pittsburgh PA, USA, Sept. 30-Oct. 4, 2007, No. 117 (2007).
10. Y. Sagayama, J. L. Carbonnier and S. Golub, "International Project Harmonization for SFR Development", *Proc. of the GIF Symposium*, Paris, France, Sept. 9-10 2009, 223-230 (2009).
11. M. Vinokur, "An Analysis of Finite-Difference and Finite Volume Formulations of Conservation Laws", NASA Contractor Report 177416, (1986).
12. A. J. Chorin, "Numerical Solution of the Navier-Stokes Equations", *Math. Comput.*, **22**, 745-762 (1968).
13. J. Smagorinsky, "General circulation experiments with primitive equation", *Monthly Weather Review*, **91**, 99-164, (1963).
14. Y. Morinishi and T. Kobayashi, "Large Eddy Simulation of Complex Flow Fields", *Computers & Fluids*, **19**(3/4), 335-346 (1991).
15. L. Temmerman, et al., "Investigation of Wall Function Approximations and Subgrid-Scale Models in Large Eddy Simulation of Separated Flow in a Channel with Streamwise Periodic Constrictions", *Int. J. Heat and Fluid Flow*, **24**, 157-180 (2003).
16. J. Gullbrand, F. T. Chow, "The effect of numerical errors and turbulence models in large-eddy simulations of channel flow with and without explicit filtering", *J. Fluid Mech.*, **495**, 323-341 (2003).
17. M. Tanaka, et al., "Numerical Investigation of Thermal Striping near Core Instruments Plate around Control Rod Channels in JSFR", *Proc. of NURETH-13*, Kanazawa, Japan, Sept. 27-Oct. 2, N13P1190 (2009).
18. H. Kamide, et al., "Study on mixing behavior in a tee piping and numerical analyses for estimation of thermal striping", *Nucl. Eng. Des.*, **239**, 58-67 (2009).
19. N. Kimura, et al., "Study on Convective Mixing for Thermal Striping Phenomena - Experimental Analyses on Mixing Process in Parallel Triple-Jet and Comparisons between Numerical Methods -", *Proc. of ICONE9*, Nice, France, April 8-12, No.4 (2001).
20. T. Kajishima, et al., "High-Order Finite Differential Method for Incompressible Flows", *Trans. of JSME, B* **63**(614), 3247-3254 (1997). [in Japanese]
21. H. K. Myong, N. Kasagi and M. Hirata, "Numerical Prediction of Turbulent Pipe Flow Heat Transfer for Various Prandtl Number Fluids with the Improved $k-\varepsilon$ Turbulence Model", *JSME Series II*, **32**(4), 613-621 (1989).
22. M. Tanaka, "Investigation of V&V process for thermal fatigue issue in a sodium cooled fast reactor - Application of uncertainty quantification scheme in verification and validation with fluid-structure thermal interaction problem in T-junction piping system", *Nucl. Eng. Des.*, **279**, 91-103 (2014)
23. M. Tanaka and Y. Miyake, "Numerical Investigation on Thermal Striping Phenomena in A T-Junction Piping System", *Proc. of the ICONE22*, Prague, Czech, July 7-11 2014, ICONE22-30683 (2014).
24. N. Nouali and A. Mataoui, "Analysis of steady turbulent triple jet flow with temperature difference", *Nucl. Eng. Des.*, **280**, 8-20 (2014).